GAP-98-035, Auger project technical note. Shower Model Comparison I : Longitudinal profile

C. Pryke
Enrico Fermi Institute, University of Chicago, USA
email: pryke@hep.uchicago.edu

December 3, 1999

Abstract

A detailed study of simulated airshower longitudinal profiles is presented. The possible influence of zenith angle is investigated, and an appropriate thinning level for the calculations is empirically determined. Simulation results are provided over a wide energy range ($10^{14.0}$ to $10^{20.5}$ eV), using four combinations of framework program & high energy hadronic interaction model, and with proton and iron primaries. The way in which the first interaction controls X_{max} is investigated, and comparisons are made to some existing experimental data.

1 Introduction

As the energy of the primary particle increases the longitudinal distribution of the resulting air shower cascade becomes smoother. At an energy of $\sim 10^{14}$ eV the depth of shower maximum X_{max} becomes a well defined quantity for showers initiated by protons and nuclei. It is also around this energy that the extensive particle showers become detectable at ground level, and coincidently, that direct detection of the primaries by satellite and balloon becomes impractical due to the decreasing flux.

Tag name	Program frame	High E Hadronic	Low E Hadronic	Electromag.
mocspl	MOCCA	Internal	Internal	Internal
mocsib	MOCCA	Sibyll	Internal	Internal
corsib	CORSIKA	Sibyll	GEISHA	EGS4
corqgs	CORSIKA	QGSjet	GEISHA	EGS4

Table 1: Summary of the four program-frame / interaction-model combinations investigated in this paper.

The longitudinal profile of air showers is of great experimental interest. In the energy range 10^{14} to 10^{16} eV it has been measured with varying degrees of directness using ground particle detectors, and also using Čerenkov light [1, 2]. The range 10^{17} to 10^{19} eV has been observed rather directly by the Fly's Eye detector through fluorescence light [3]. Finally the region above 10^{19} eV is the focus of the HiRes Fly's Eye [4], Auger Project [5] and others.

Simulations of air showers usually focus on a narrow energy range of interest to a particular experiment. This is unfortunate since checking the consistency of experiments in adjacent energy ranges is critically important given the uncertainty of the high energy hadronic interaction models.

A technique called thinning is used to dramatically accelerate the simulation of air shower cascades. Below a threshold level only a sub-set of the particles are tracked, with weightings to compensate for those discarded. The threshold is usually specified as a fraction of the primary energy, and referred to as the "thinning level".

When considering gross quantities like the longitudinal profile of all charged particles it is possible to run the simulation codes with very severe thinning and still obtain high quality results. This means that many showers can be generated over a multidimensional grid of primary parameters and shower models within an acceptable computing time.

In this paper four combinations of framework program and high energy hadronic interaction model are investigated; these are summarized in table 1. The "tag names" will be used to refer to these throughout. Showers were generated in the energy range $10^{14.0}$ to $10^{20.5}$ eV with both proton and iron primaries.

Sections 2 and 3 address some practical details. In section 4 the choice of simulation parameters is explored. The main investigation of different models, over a wide energy range is presented in section 5. The behavior of the first interaction and its influence on shower development is investigated in section 6. In section 7 X_{max} is considered in detail and the results are compared to some existing experimental data.

2 Detailed Run Conditions

CORSIKA is a well documented and thorough program prepared originally for the Kascade experiment [6]. It has the attractive feature of using the well established HEP codes EGS4 [7] and GEISHA [8] for the lower energy modeling, thus hopefully keeping the uncertainty in the high energy hadronic model where it is unavoidable. This is of considerable advantage when dealing with the psychology of sceptical outsiders to the air-shower field. Version 5.620 of CORSIKA was used (3 April 1998); this includes a very similar thinning algorithm to MOCCA, and the LPM effect is correctly implemented [9].

MOCCA is a much less well documented and maintained program written by Michael Hillas [12]. It was the first such program to implement thinning, and has been used extensively by several groups. The so-called "Michigan version" of MOCCA-Sibyll was used dating from approximately 1992.

For details of the Sibyll and QGSjet models see [10, 11]. In all cases the high energy hadronic interaction model was used with the set of inelastic cross sections provided by it's authors. Electromagnetic particle energy cutoff was a uniform 0.2 MeV.

Known differences between the run conditions are as follows:

- In CORSIKA the transition between the High Energy and Low Energy interaction model (GEISHA) and cross sections takes place at 80 GeV. In MOCCA the corresponding threshold was set to 200 GeV This is expected to make a negligible difference.

- The version of Sibyll used with MOCCA was 1.5; with CORSIKA it was 1.6.

3 Longitudinal Profile Fitting

The simulation programs record the number of charged particles crossing "census" planes spaced at 10 g cm^{-2} intervals of vertical atmospheric depth.

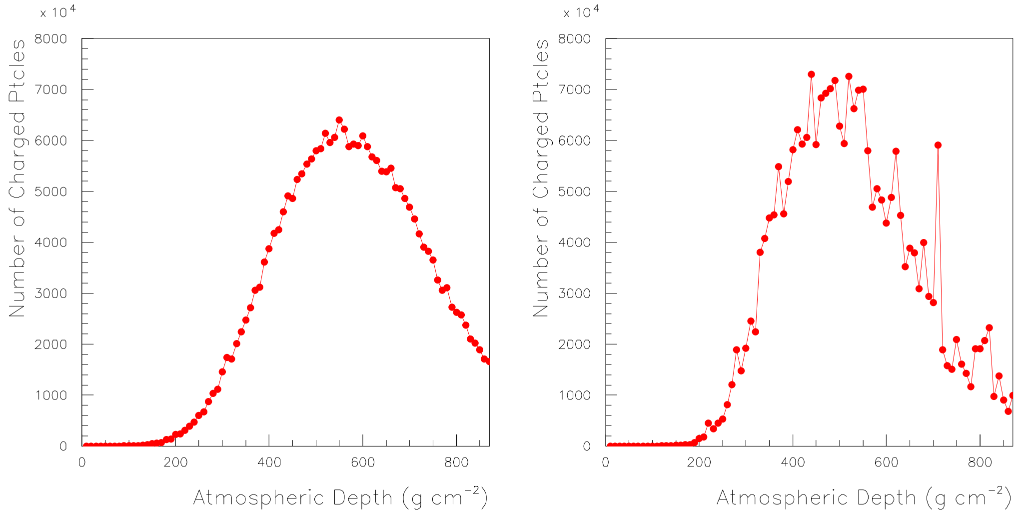

Figure 1: The longitudinal profiles of two simulated showers. At left the thinning level is $10^{-5.5}$ of primary energy, and at right $10^{-3.5}$. (**corsib**, proton, 10^{17} eV, 45 deg.)

Ground level was placed at 870 g cm^{-2} vertical depth in all cases. The resulting longitudinal profiles are fit as follows.

3.1 Thinning, weighting and goodness of fit

The process of thinning produces longitudinal profiles which have large non-statistical fluctuations. The magnitude of these fluctuations increases with the severity of the thinning. Figure 1 shows the longitudinal profiles of two showers with the same primary parameters, but different thinning levels.

For a thinned longitudinal profile the rms dispersion of the $N(X)$ values about a best fit line turns out to be proportional to $\sqrt{N(X)}$, the constant of proportionality increasing with increasingly severe thinning. We weight the points according to this rule in all fits.

To generate a "goodness of fit" parameter we calculate a conventional χ^2/ndf with the $\sqrt{N(X)}$ weightings mentioned above. The resulting numbers are of course very large, but are useful for comparative purposes.

3.2 Fitting function

The following function was introduced by Gaisser and Hillas [13] as a "simple analytic parameterization" of the longitudinal profile of air showers:

$$N(X) = N_{max} \left(\frac{X}{X_{max}} \right)^{X_{max}/\lambda} \exp\left(X_{max} - X\right)/\lambda, \tag{1}$$

where X is the atmospheric depth (in g cm^{-2}), N_{max} is the number of cascade particles at shower maximum, X_{max} is the depth of maximum, and λ is a characteristic length parameter (taken to be 70 g cm^{-2}). This function has the same shape as a Gamma Function, a form which naturally arises in cascade theory. It is a fairly good fit to simulated cascade profiles.

A fourth parameter is often introduced into equation 1,

$$N(X) = N_{max} \left(\frac{X - X_0}{X_{max} - X_0} \right)^{(X_{max}-X_0)/\lambda} \exp\left(X_{max} - X\right)/\lambda, \tag{2}$$

where X_0 is sometimes stated to be the first interaction point. Even if this were the case the function would be inelegant in that varying X_0 does not correspond to a translation along the X axis unless X_{max} is also changed. In fact it turns out that X_0 correlates poorly with the actual depth of first interaction, and frequently takes negative values — see figure 2.

Experiments were made performing the fit with X_0 fixed at the actual depth of the first interaction. This produces a significantly poorer goodness of fit, and reduces the X_{max} results by $\leq$ 10 g. For the remainder of this paper equation 2 was used with all four parameters free. However note that X_0 is best regarded as simply an additional arbitrary shape parameter, and is not to be confused with the actual depth of the first interaction which will later be called X_1.

Note that when using equations 2 it is necessary to force $N(X) = 1$ when $X < X_0$.

4 Choosing the Simulation Parameters

Since we cannot investigate an infinite parameter space we must choose a thinning level and zenith angle at which to conduct the main investigation. In section 4.1 it is demonstrated that a thinning level of $10^{-4.5}$ is adequate when making parametric fits of simulated longitudinal profiles. It is often

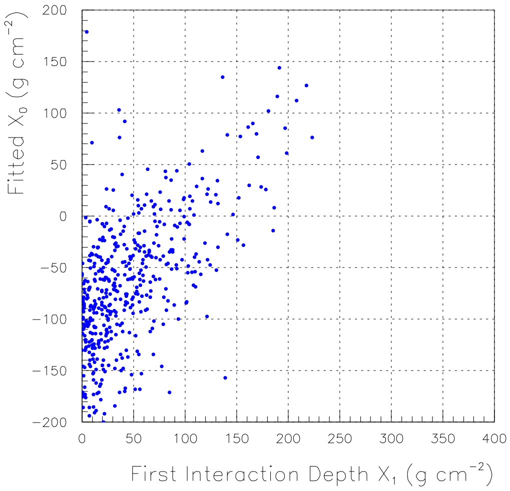

Figure 2: The fitted value of X_0 versus the actual depth of first interaction for a set of 500 **corsib** proton showers at 10^{17} eV. The result is qualitatively the same for all models, primaries and energies.

assumed that the development of an air shower cascade is controlled only by the mass of atmospheric material through which it has passed. This assumption is checked in section 4.2. These checks are conducted in the middle of the energy range of the main investigation at 10^{17} eV.

4.1 Varying the thinning level

To determine the thinning level required to produce profiles of adequate quality for this study sets of 500 showers were generated at each of 5 thinning levels; $10^{-3.5}$, $10^{-4.0}$, $10^{-4.5}$, $10^{-5.0}$, and $10^{-5.5}$. **corsib** was used with the following primary parameters; proton, 10^{17} eV, 45 deg zenith angle.

The profiles were fit to equation 2, with all four parameters free. Figure 3 shows the goodness of fit versus thinning level.

Figure 4 shows the distributions of the fit parameters at the 5 thinning levels; they are clearly very similar. To test further we take the $10^{-5.5}$ thinned distributions as reference and perform a Kolmogorov test [1] against each of the more heavily thinned sets, for each of the parameters. This is a statistical test of the compatibility in shape between two histograms — it yields the

[1]The test as implemented in the HBOOK function HDIFF [14] was used.

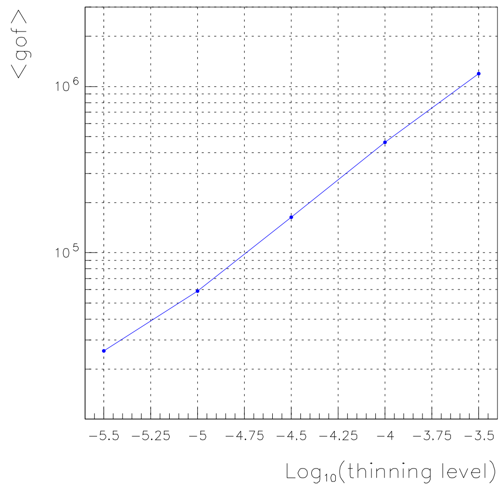

Figure 3: Goodness of fit versus thinning level.

probability that they are drawn from the same parent distribution.

All the fit parameters return a high probability at thinning levels of $10^{-5.0}$, and $10^{-4.5}$. This indicates that within the statistics of a 500 event set the results are indistinguishable from $10^{-5.5}$ thinning. At $10^{-4.0}$, and $10^{-3.5}$ the probabilities become very small indicating that the increasingly severe thinning is biasing the results. Given the desire for the quickest possible run time, a thinning level of $10^{-4.5}$ was selected for the main study.

4.2 Varying the Zenith Angle

As an air shower develops in the upper atmosphere various processes compete. The probability for interaction depends on the mass of material traversed. The probability for decay depends on the time elapsed. For a relativistic particle the ratio of these depends on the density of the air, which, of course, increases approximately exponentially moving downward through the atmosphere.

A primary which arrives at a large zenith angle initiates a cascade which spends more time in the less dense upper levels of the atmosphere. This might alter the cascade as compared to a more vertical one, for instance by favoring charged pion decay over re-interaction, leading to an increased fraction of the primary energy going into the muon channel, and depressing N_{max}.

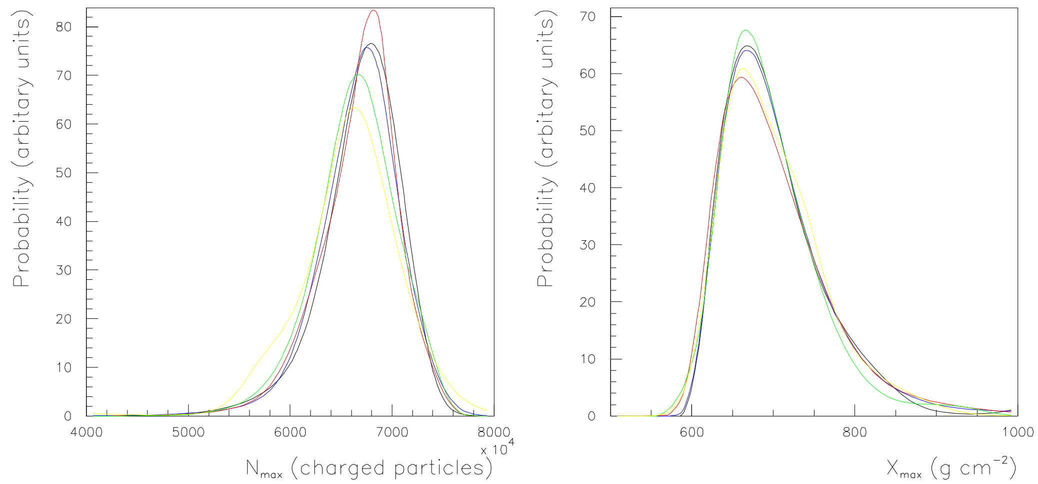

Figure 4: Distributions of N_{max} and X_{max} for sets of 500 showers each at 5 thinning levels between $10^{-5.5}$ and $10^{-3.5}$ of primary energy. The lowest thinning level is the darkest line (black), and increasingly light colored lines correspond to increasing thinning (blue, red, green, yellow).

It is normally assumed that such effects are not important, and that cascades will develop identically at any zenith angle when the longitudinal parameter considered is air mass traversed (measured in g cm^2). To test this assumption sets of 500 showers were generated at each of 5 zenith angles; 0, 37, 48, 55 and 60 deg. When considering the "stretching" of the atmospheric density profile the relevant quantity is $\sec\theta$; these zenith angles correspond to values of 1.00, 1.25, 1.50, 1.75, and 2.00. **corsib** was used with the following primary parameters; proton, 10^{17} eV, $10^{-4.5}$ thinning level.

In all simulations in this paper particles are tracked to ground level placed at 870 g cm^{-2}. At high energy vertical events are not far past maximum at this depth, and hence only the leading edge of the longitudinal profile is available to fit. In this section we restrict the fit range to the first 870 g cm^{-2} of slant depth at all zenith angles. This distorts the results, but ensures comparability between the different zenith angle sets [2]

[2]It would of course be possible in simulation to track particles to an arbitrary atmospheric depth, and provide complete cascade profiles at all zenith angles. However, experimentally the ground always gets in the way! Hence, in the context of the check being performed here, it makes at least as much sense to truncate the fit range for the large angle profiles.

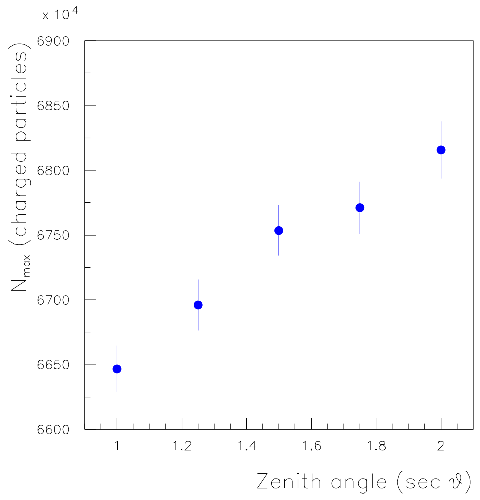

Figure 5: Correlation of mean N_{max} with shower zenith angle.

Each set of profiles was again fit to equation 2, with all four parameters free. Applying the Kolmogorov test with the central $\sec\theta = 1.50$ set as reference we find that X_{max} and λ return an acceptable probability for all zenith angles. However N_{max} fails at $\sec\theta = 1.00$ and $\sec\theta = 2.00$ (probability $\ll 0.01$). Figure 5 shows why this is so; the mean value of N_{max} increases with zenith angle. The change is 2.5% over the range considered. It is an interesting question why N_{max} increases, rather than decreasing as would be expected from the simple argument above.

A zenith angle of 45 deg was selected for the main study ($\sec\theta = 1.41$).

5 Varying the Primary Energy and Shower Model

Sets of 500 events were run at 14 half decade energy steps between 10^{14} and $10^{20.5}$ eV, with the 4 combinations of framework program and high energy hadronic interaction model given in table 1. Sets were generated with both proton and iron nucleus primaries. This gives $500 \times 14 \times 4 \times 2 = 56,000$ showers. The showers were run at a thinning level of $10^{-4.5}$ of primary energy, and a zenith angle of 45 deg. The number of charged particles crossing planes spaced every 10 g cm^{-2} of vertical depth (14.1 g cm^{-2} slant) were recorded, and ground level placed at 870 g cm^{-2} vertical depth (1230 g cm^{-2} slant). The resulting profiles were fit to equation 2 with all four parameters free, the fit being made over the full range of X in all cases [3]

In the following plots the width of the bands are estimated errors on the assumption of normally distributed data (ie. errors on mean and σ of $\sigma/\sqrt{n}$ and $\sigma/\sqrt{2n}$ respectively).

5.1 X_{max}

Figure 6 shows the mean and standard deviation (σ) of X_{max}, plotted against energy over the complete range. **mocsib** and **corsib** proton results are in good agreement, as we expect, since this parameter should be primarily determined by the high energy hadronic model. Despite the differing treatment of nuclear fragmentation in these two cases the results for iron are also close. At higher energies the older **mocspl** model diverges strongly to deeper X_{max}, while **corqgs** produces much shallower results; so much so that at $10^{20.5}$ eV **mocspl** iron is equal to **corqgs** proton.

The standard deviation of X_{max} is plotted as its absolute value in g cm^{-2}. There is no significant difference between the models except for **corqgs** with proton primaries where the values are somewhat greater at higher energies. Since the difference between the mean X_{max} for proton and iron is also smaller for **corqgs**, this implies that differentiating between heavy and light primaries experimentally will be more difficult under this model.

5.2 N_{max}

Figure 7 shows the mean and standard deviation (σ) of N_{max}, plotted against energy. The relationship between N_{max} and E is close to linear and so is plotted in the form mean N_{max}/E where E is in GeV. At lower energies proton primaries are more efficient at producing charged particles since a larger fraction of the available energy goes into the electromagnetic cascade.

[3]Since X_{max} increases with energy and the cascade profiles are cut off at ground level a reducing portion of the complete cascade profile is available to fit. As noted in section 4.2, fitting a function which may not perfectly describe the cascade shape to a different section of the profile could bias the results. To check for this each profile was fit again using the portion between the top of the atmosphere and 150 g beyond an initial estimate of X_{max}. The systematic change in mean X_{max} was < 6 g in all cases so we choose to ignore this effect.

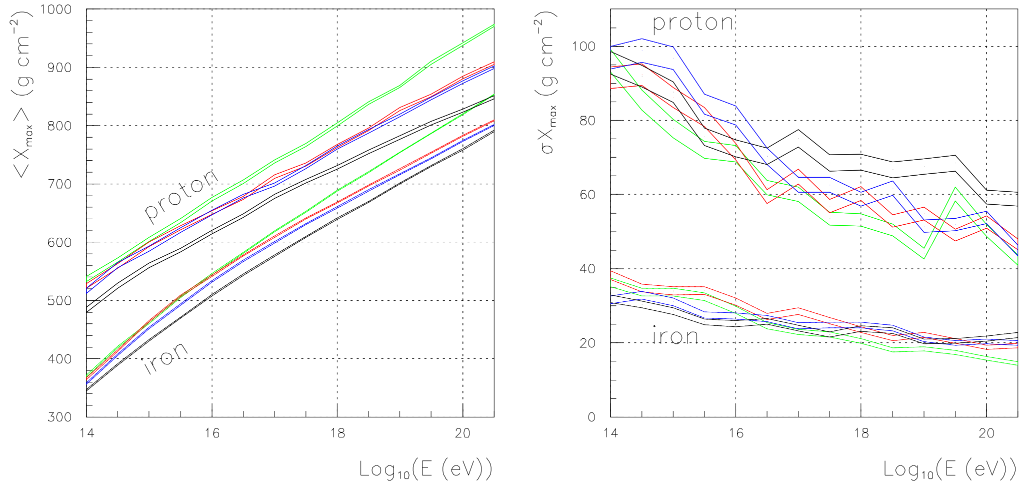

Figure 6: The depth of shower maximum X_{max} versus energy for four combinations of framework program and high energy hadronic interaction model, and proton and iron primaries. Increasingly dark lines correspond to **mocspl**, **mocsib**, **corsib** and **corqgs** (green, red, blue, black).

At higher energies proton and iron curves converge as the electromagnetic fraction approaches 100%. However, at the highest energies the proton curves dip below the iron; this seems unexpected, and must be connected with a change in shape of the proton cascade, possibly connected with the LPM effect.

A second thing to note is that the difference between MOCCA and CORSIKA at high energy is much larger than between the two high energy hadronic models of each program. CORSIKA gives $\sim 10\%$ fewer particles at maximum, and since it incorporates the well established EGS4 electromagnetic cascade model, is presumably closer to the truth.

The standard deviation of N_{max} is plotted as a fraction of the mean, and is 5% at the highest energies for proton, and a little less for iron. All models give similar results.

5.3 Shape Parameters λ and X_0

Figure 8 shows the mean and standard deviation (σ) of λ and X_0, plotted against energy. The width of the longitudinal profile is controlled by a combination of these two and the fitting algorithm finds the assigned values to

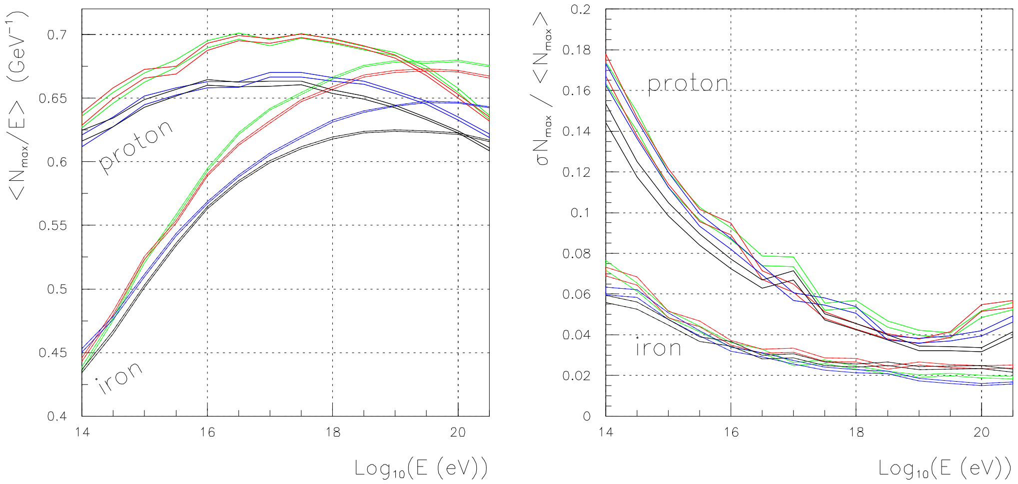

Figure 7: Number of charged particles at shower maximum N_{max} versus energy for four combinations of framework program and high energy hadronic interaction model, and proton and iron primaries. Increasingly dark lines correspond to **mocspl**, **mocsib**, **corsib** and **corqgs** (green, red, blue, black).

be highly correlated. Note that the tendency to select negative values of X_0 does not depend on the shower model, or primary type, but does increase with energy.

5.4 Goodness of Fit

Figure 9 shows the mean goodness of fit plotted against energy. To allow comparison at different energies the values are divided by N_{max}. Note that CORSIKA yields equal results for both hadronic models and primary types. As expected the goodness of fit improves with energy, since the longitudinal profile shape becomes better defined and more repeatable. The behaviour of MOCCA seems harder to understand.

6 Influence of the First Interaction on X_{max}

Why does X_{max} differ between the models as shown in figure 6? It turns out that most of the difference can be understood in terms of the position and character of the first interaction.

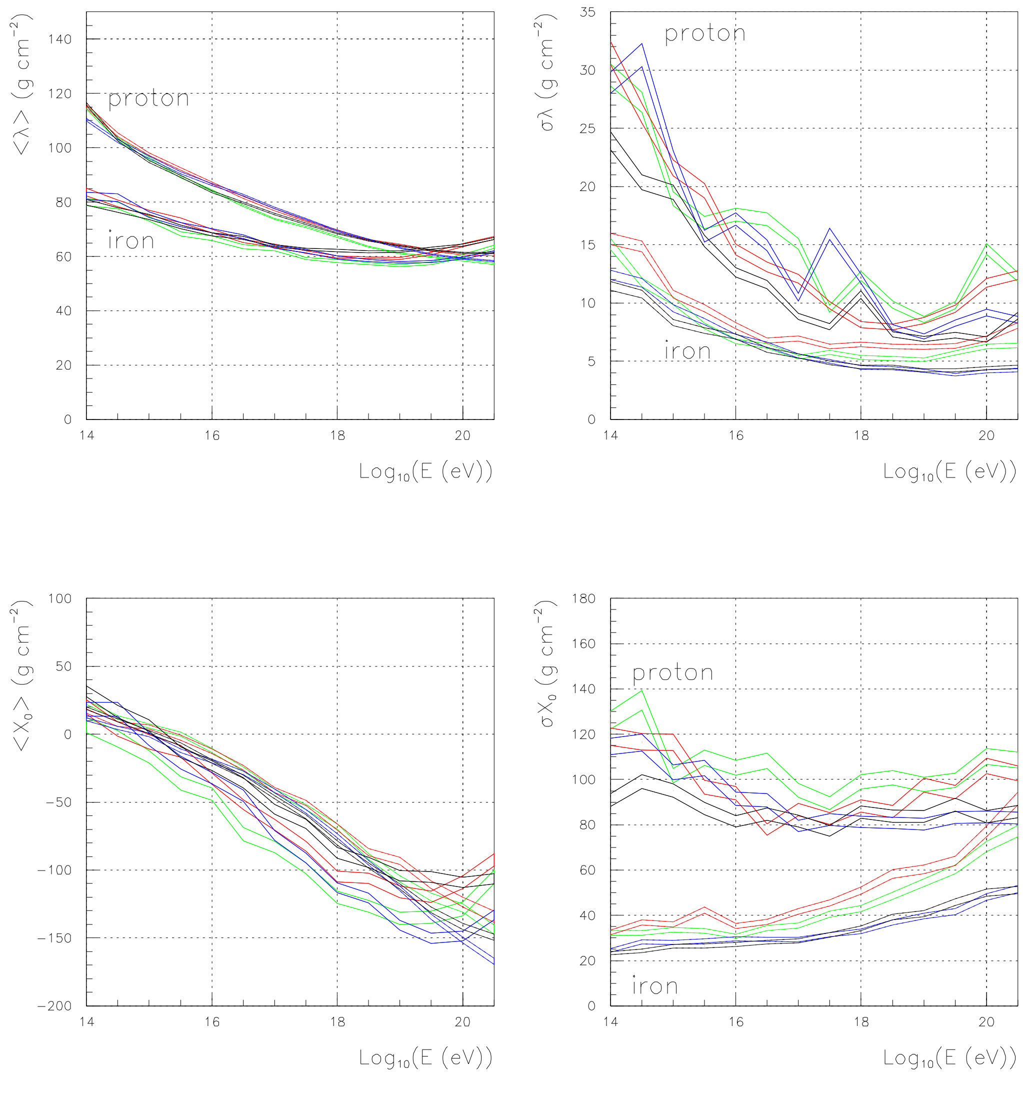

Figure 8: Longitudinal profile shape parameters λ and X_0 versus energy for four combinations of framework program and high energy hadronic interaction model, and proton and iron primaries. Increasingly dark lines correspond to **mocspl**, **mocsib**, **corsib** and **corqgs** (green, red, blue, black).

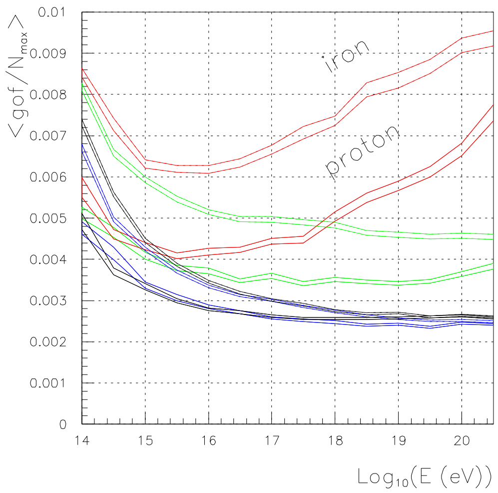

Figure 9: Mean goodness of fit versus energy for four combinations of framework program and high energy hadronic interaction model, and proton and iron primaries. Increasingly dark lines correspond to **mocspl**, **mocsib**, **corsib** and **corqgs** (green, red, blue, black).

6.1 First Interaction Depth, X_1

Figure 10 shows the mean value of X_1 plotted against energy. This is the mean free path of the primary cosmic rays and necessarily has an exponential distribution. The differences between the models for proton primaries are not large. As expected **mocsib** and **corsib** are the same; **corqgs** is similar, and **mocspl** is about 10 g cm^{-2} less at high energies. However, the extrapolation from proton-air to nucleus-air cross sections seems to be different in MOCCA and CORSIKA, with the MOCCA mean free paths being almost twice as long at low energy.

6.2 Elasticity

When investigating the way in which the first interaction controls the depth of shower maximum X_{max} it is natural to subtract out the position of the first interaction; $X_{rise} = X_{max} - X_1$. It is this quantity which we expect the correlate with properties of the first interaction, since it is the distance after initiation which the shower takes to reach maximum.

It turns out that the difference in X_{rise} between Sibyll and QGSjet is a

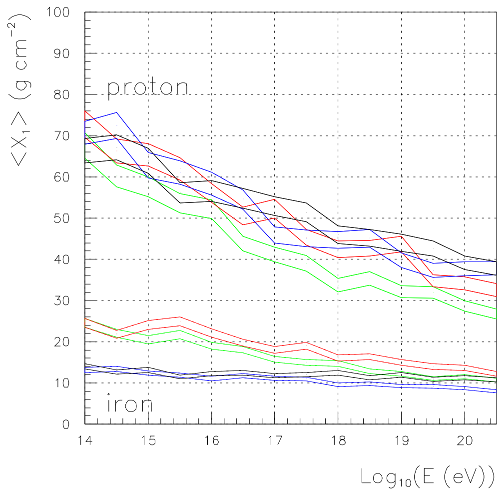

Figure 10: Mean free path versus energy for four combinations of framework program and high energy hadronic interaction model, and proton and iron primaries. Increasingly dark lines correspond to **mocspl**, **mocsib**, **corsib** and **corqgs** (green, red, blue, black).

consequence of the differing elasticity distributions produced by those models. Elasticity is defined as the energy fraction of the most energetic secondary. Normally a large fraction of the primary energy continues in the form of a "leading nucleon" and the remainder is split between many secondary nucleons and pions.

Figure 11 shows that the elasticity of the first interaction is highly correlated with X_{rise}. This is expected; if the first interaction is catastrophic the resulting shower takes fewer generations to reach maximum. Both models appear to give the same relationship between elasticity and X_{rise} implying that elasticity is the primary factor controlling shower development. As elasticity becomes larger the importance of the first interaction in determining the subsequent shower development becomes less and the correlation becomes poorer.

It is hence interesting to investigate elasticity further. Figure 12 shows some plots of elasticity for **corsib** and **corqgs** proton-air interactions. The upper left frame shows the quantity most often considered — the mean elasticity versus energy. The two models give similar results. However, this is misleading; the upper right frame shows the elasticity distributions at

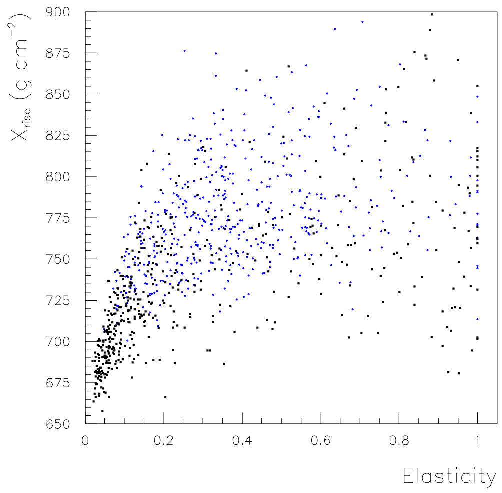

Figure 11: The correlation of X_{rise} with first interaction elasticity for primary protons at 10^{19} eV. Light points are **corsib** and darker **corqgs** (blue and black).

10^{19} eV, and these are sharply different. QGSjet produces many more very hard events where the highest energy particle emerging carries $< 10\%$ of the primary energy. The lower two frames of the figure show the elasticity distributions versus energy. Note that Sibyll has rather constant behaviour, while QGSjet is a more radical model showing a stronger change with energy.

Multiplicity is highly correlated with elasticity as shown in figure 13. It is therefore not worthwhile to seek additional correlations such as X_{rise} versus multiplicity.

7 X_{max} and How to Use It

The distance from the top of the atmosphere to shower maximum is an experimentally observable quantity, and therefore of great interest. In the following section various ways to consider X_{max} data are discussed.

7.1 Mean

The mean X_{max} data produces adequate χ^2/ndf when fit by a cubic polynomial. To facilitate use of the current results in future work table 2 gives the

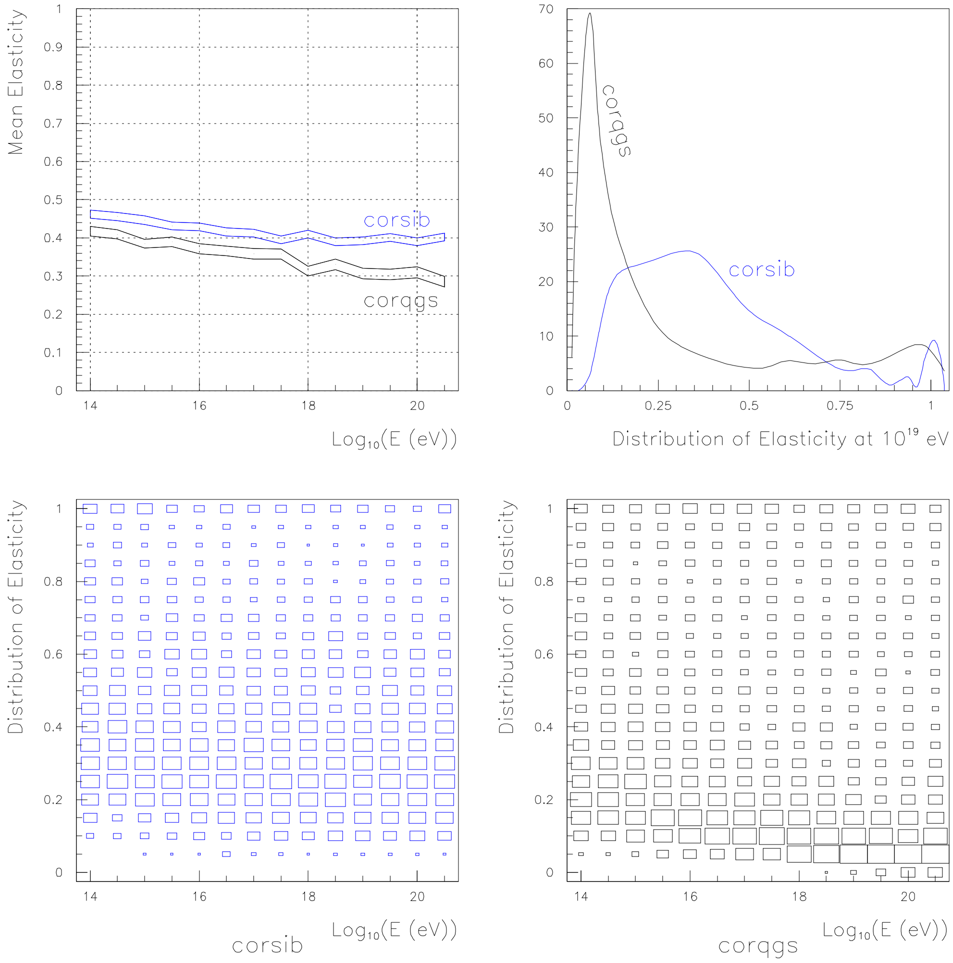

Figure 12: Plots of elasticity — see text for explanation. In the lower two plots the *side length* of the boxes is proportional to the bin contents.

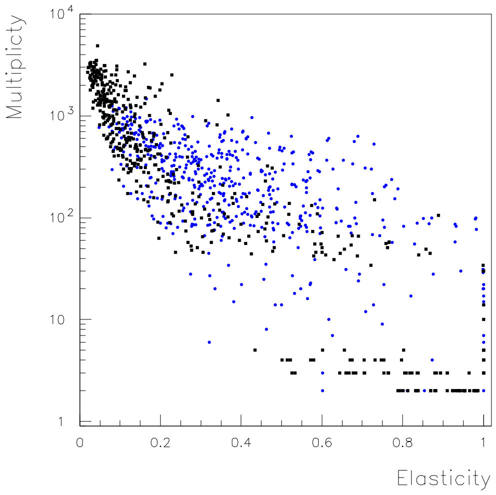

Figure 13: The correlation of first interaction multiplicity with elasticity for primary protons at 10^{19} eV. Light points are **corsib** and darker **corqgs** (blue and black).

coefficients of $X_{max}(e) = c_0 + c_1 e + c_2 e^2 + c_3 e^3$, where $e = \log_{10}(E(eV))$. A table of raw values is given in appendix A.

An encouraging feature is that all models are close to agreement at 10^{14} eV, as they presumably should be since this energy range is fairly well understood from accelerator experiments.

The crudest way to compare experimental X_{max} data with shower simulations is to consider the mean value of X_{max}. This is what the most commonly shown Fly's Eye plot does [3, fig. 3], and it is claimed to show evidence of a transition from a heavy dominated to a light dominated composition over the energy range $10^{17.5}$ to 10^{19} eV.

Figure 14 shows a comparison between published X_{max} data from several experiments and the four combinations of framework program and high energy hadronic interaction models. The data for $E < 10^{16}$ eV are from the DICE experiment [1], and for $E > 10^{17}$ eV from the Fly's Eye [3]. The point near 10^{14} eV is an estimate based on direct composition measurements [1].

The Fly's Eye data contains an un-corrected experimental bias. The approach followed by that group is to process simulated longitudinal profiles through a detector Monte-Carlo and reconstruct the results using their usual algorithms. Hence they compare biased simulated data with un-corrected

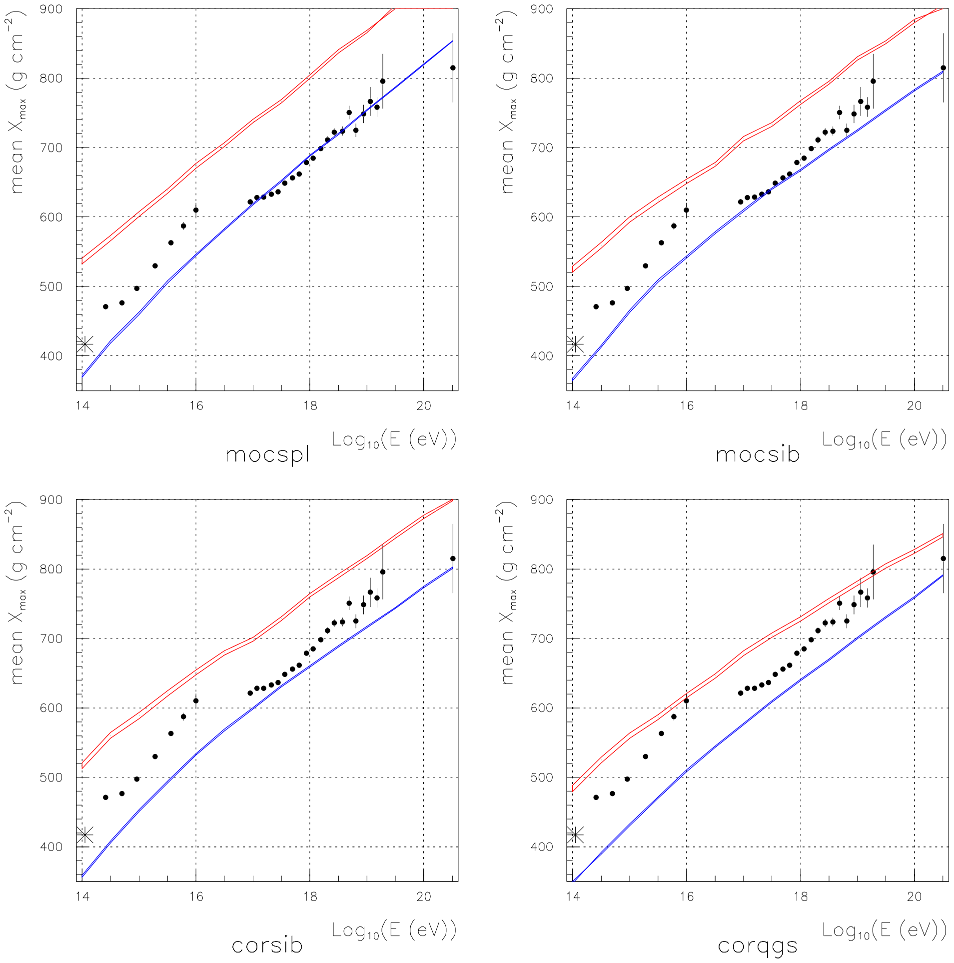

Figure 14: A Comparison of experimental mean X_{max} data with four combinations of framework program and high energy hadronic interaction model.

Tag name	primary	c_0	c_1	c_2	c_3
mocspl	p	-0.964E+03	0.169E+03	-0.611E+01	0.121E+00
	fe	-0.352E+04	0.545E+03	-0.253E+02	0.445E+00
mocsib	p	-0.141E+04	0.248E+03	-0.106E+02	0.196E+00
	fe	-0.543E+04	0.870E+03	-0.434E+02	0.769E+00
corsib	p	-0.229E+04	0.399E+03	-0.192E+02	0.356E+00
	fe	-0.479E+04	0.757E+03	-0.369E+02	0.646E+00
corqgs	p	-0.180E+04	0.288E+03	-0.115E+02	0.181E+00
	fe	-0.334E+04	0.515E+03	-0.238E+02	0.413E+00

Table 2: Cubic polynomial fit parameters of mean X_{max} for four combinations of framework program and high energy hadronic interaction model, and proton and iron primaries.

real data. This makes it very difficult for an outsider to use the published results.

In [15, sec. D] there is a discussion of the detector bias effects. At 10^{18} eV the more penetrating proton initiated showers are biased deeper by ~ 10 g cm^{-2}, while the shallower iron showers shift deeper by ~ 20 g cm^{-2}. Presumably the bias is X_{max} and energy dependent [16, sec. 4, par. 2, scent. 2]. If this is the case the experimental data could be corrected using the simulations as a guide. It is only if the bias is specifically composition dependent — for instance through the shape of the profile — that the Fly's Eye procedure seems to be justifiable.

Simple minded comparison of the Fly's Eye data with **mocspl** would indicate a very heavy composition over their entire energy range; however, this model should probably not be taken seriously. The other models all indicate some trend to a lighter composition mix, but the extent of the change is far less dramatic than in the original KNP model plot [3, fig. 3]. Introducing a bias to shallower X_{max} in the lower energy data points would slightly increase the magnitude of the implied composition change [16, fig. 1]. Without a better estimate of the uncorrected experimental bias it is impossible to say more.

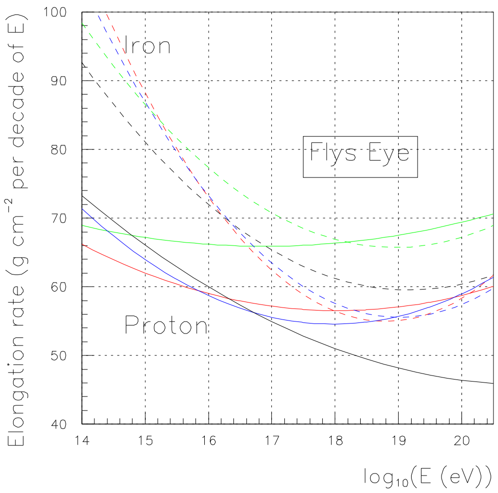

Figure 15: Elongation rate versus energy for four combinations of framework program and high energy hadronic interaction model, and proton and iron primaries. Increasingly dark lines correspond to **mocspl**, **mocsib**, **corsib** and **corqgs**(green, red, blue, black).

7.2 Elongation Rate

The rate of change of mean X_{max} with $\log_{10}(E)$ is often called the Elongation Rate. This quantity is much less subject to systematic error than the absolute value of mean X_{max}. Using the data given in table 2 we can plot $dX_{max}/de = c_1 + 2c_2 e + 3c_3 e^2$, where $e = \log_{10}(E)$ in eV. Figure 15 shows the result. The Fly's Eye group find that the elongation rate from 3×10^{17} to 1×10^{19} eV is 78.9 ± 3 g cm^{-2} [17]; this is indicated on the figure, and is clearly inconsistent with a constant composition for all models considered here.

7.3 Standard Deviation

Attempts have also been made to compare the standard deviation of X_{max} to experimental data. Figure 16 shows a comparison between published X_{max} data from several experiments and the four combinations of framework program and high energy hadronic interaction models. The data for $E < 10^{16}$ eV are from the AIROBIC experiment [2], and for $E > 10^{17}$ eV from Fly's Eye [18]. These points have an uncorrected bias due to experimental resolution. However they clearly rule out an exclusively heavy composition.

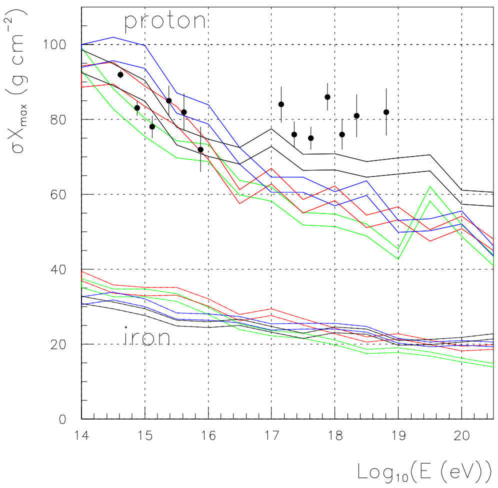

Figure 16: A Comparison of experimental standard deviation of X_{max} data with four combinations of framework program and high energy hadronic interaction model.

7.4 X_{max} Band Plot

The overlap of the proton and iron X_{max} distributions as predicted by the various models is interesting. This is shown in Figure 17 where the bands contain 68% of the data (ie. 16% and 84% points of the integral distribution). Notice that the models are quite different when viewed in this way; **mocspl** shows strong separation improving with increasing energy, while **corqgs** has weaker separation degrading with energy.

There has been some discussion of using cuts on a composition sensitive parameters to extract a proton rich sub-set of the Auger data for point source and anisotropy studies. This would clearly work much less well if QGSjet is a more realistic model than Sibyll.

7.5 X_{max} Distribution Shape

The standard deviation of X_{max} is an inadequate representation of the spread of this parameter. The distribution is asymmetric, with a tail to deep X_{max}. It is easy to understand why: X_{max} is the sum of X_0 and X_{rise}. X_0 has an exponential distribution, whilst X_{rise} is *approximately* Gaussian. The distribution of X_{max} is simply the convolution of these two. Within the

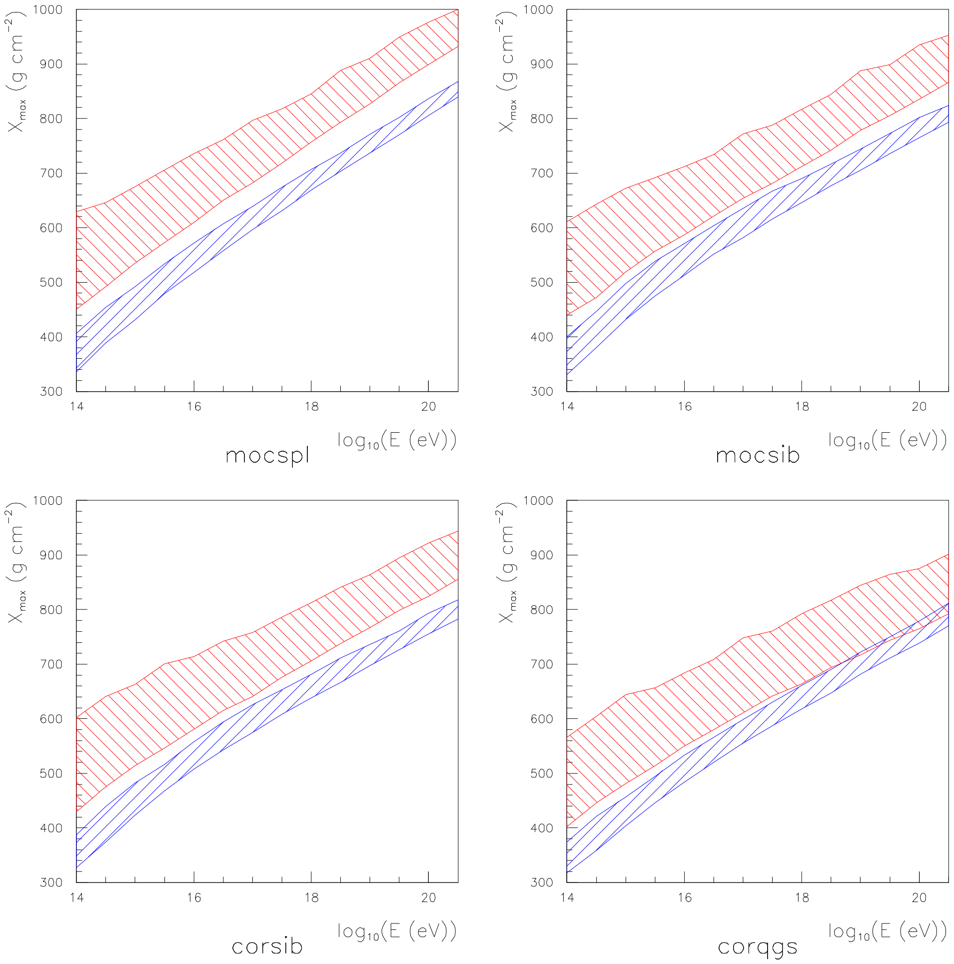

Figure 17: The distribution of X_{max} versus energy shown as a band containing the central 68% of the data. The upper band in each case is proton primaries, and the lower iron. Four combinations of framework program and high energy hadronic interaction model are plotted.

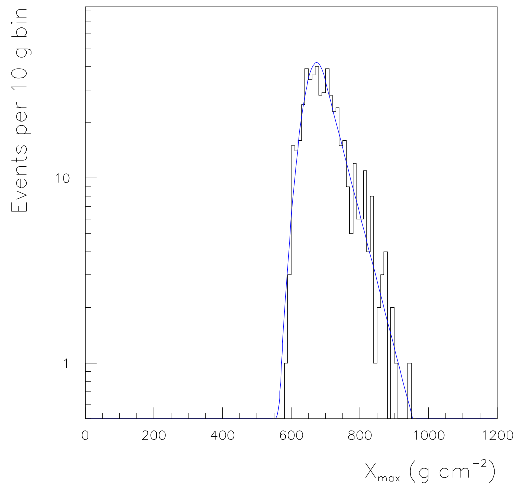

Figure 18: The distribution of X_{max} for **corsib** protons at 10^{17} eV. The curve is the Gaussian/Exponential fit described in the text.

statistics of a 500 shower set it can be adequately fit by a Gaussian joined to an exponential at transition point (t);

$$\begin{array}{ll} X_{max} < t; & f_1 = c \exp\left(\frac{(X_{max}-X_{peak})^2}{2\sigma^2}\right) \\ X_{max} > t; & f_2 = f_1(t)\exp(-d(X_{max}-t)) \end{array} \tag{3}$$

The fitted value for t is typically $X_{peak} + 0.5\sigma$. Figure 18 shows an example fit. It is interesting to note that the iron-primary distributions also require an exponential tail to produce an adequately good fit — it might have been expected that they would be close to purely Gaussian. To get accurate values for σ and d it is essential to make these fits using a maximum likelihood algorithm since the bins on the exponential tail necessarily contain few events.

Attempts have been made to use the back edge of the X_{max} distribution to obtain information about the proton-air cross section at ultra high energies, and by extrapolation, the proton-proton cross section. This is a quantity of fundamental interest which is unobtainable by any other means. Figure 19 shows the ratio of $1/d$ to the proton mean free path. The value is a little greater than unity across the energy range, and independent of model.

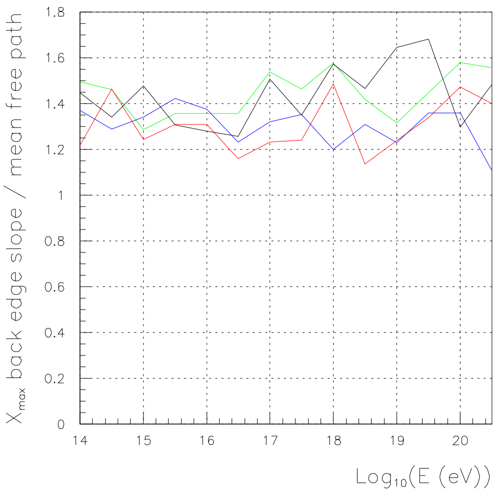

Figure 19: Ratio of the slope of an exponential fit to the back edge of the X_{max} distribution to the mean free path. Increasingly dark lines correspond to **mocspl**, **mocsib**, **corsib** and **corqgs** (green, red, blue, black).

8 N profile or E profile?

It is customary to fit the longitudinal profile of charged particle number. However fluorescence light production is proportional to energy deposition, and not particle number [19] An assumption in Fly's Eye analysis is that the vast bulk of particles are of low energy (and singly charged), and hence that the longitudinal profile of fluorescence light production has the same shape as that of charged particle number.

From version CORSIKA 5.87 (Jan. 1999) longitudinal profiles of energy deposition, as well as particle number, are recorded. To check for a possible bias **corqgs** was re-run using this version and the energy profiles fit in the same way as the particle profiles. A systematic difference in X_{max} was undetectable with 500 shower sets — it was less than a few grams.

9 Online Materials

The entire set of runs generated for this paper are available online at this time. The gzipped log files occupy 350 MB. A reduced HBOOK file is 4 MB in size. Both sets of files are available at: `ftp://aupc1.uchicago.edu` — once there proceed to the directory `auger/showlib/modcomp/longprof/pro/gap-98-035`. Putting the above address into Netscape is recommended as informational messages will display for each directory. (Once the ftp site has been explored batches of files can be downloaded with a standard ftp client.)

10 Conclusions and Recommendations for Future Work

The parameter X_0 in equation 2 correlates poorly and in a biased manner with the actual depth of first interaction when fitting simulated shower profiles. Hence X_0 and λ should be regarded simply as arbitrary shape parameters.

The process of thinning works. To study X_{max} it is better to run heavily thinned showers with explicit low energy hadronic and electromagnetic cascades than to rely on analytic approximations for these parts of the simulation. This has frequently been done in the past, and always leads to worries that these are biasing the results to an unknown extent. When working with an explicit, but thinned, cascade simulation it is possible to determine an appropriate thinning level empirically as was shown in section 4.

Thinning allows a large number of showers to be run over the complete range of experimental energies with a variety of hadronic interaction models. Without it this is simply impossible.

The way in which the first interaction controls X_{max} has been investigated. The influence is strong — if one were to use model A for the first interaction, and model B thereafter the mean X_{max} results would be close to using model A throughout.

X_{max} has been carefully calculated for four combinations of framework program and high energy hadronic interaction model, and proton and iron primaries. Polynomial fit coefficients are quoted for this data, and a table of values is provided. It is hoped that these will be of use for future comparisons with experimental data, and with other simulation results. The complete set of showers generated for this study are available for ftp download.

Ways to use X_{max} data have been investigated including mean value, elongation rate, standard deviation, "band plot", distribution shape, and distribution back edge decrement.

Finally it was checked that the longitudinal profile of energy deposition yields identical results to that of charged particle number.

It would be very useful if a common reference set of showers were made available by authors of new or modified hadronic interaction models. For the purposes of longitudinal profile comparison the set used here seems adequate.

11 Acknowledgements

The Fermilab computing department are thanked for the use of their machines. Also special thanks to the Fermilab Sloan Digital Sky Survey Group for the use of a very powerful DEC Alpha machine on which the CORSIKA showers were run.

A Table of X_{max} values

The following tables gives mean and standard deviation values of X_{max} for four combinations of framework program and high energy hadronic interaction model, and proton and iron primaries. Each pair of numbers comes from a 500 shower set.

Primary	$\log_{10} E$	X_{max}			
	(eV)	mocspl	mocsib	corsib	corqgs
Proton	14.0	537 , 96	525 , 91	517 , 97	484 , 96
	14.5	570 , 86	559 , 92	560 , 99	525 , 92
	15.0	605 , 78	597 , 86	589 , 97	560 , 88
	15.5	637 , 72	625 , 81	621 , 84	587 , 76
	16.0	674 , 71	651 , 72	651 , 81	618 , 72
	16.5	704 , 62	676 , 59	679 , 70	646 , 70
	17.0	738 , 60	713 , 65	699 , 63	679 , 75
	17.5	767 , 54	733 , 57	729 , 63	705 , 68
	18.0	802 , 53	765 , 60	762 , 59	728 , 69
	18.5	839 , 50	793 , 53	790 , 62	755 , 67
	19.0	867 , 44	829 , 55	817 , 52	779 , 68
	19.5	908 , 60	852 , 49	847 , 52	804 , 68
	20.0	940 , 50	883 , 53	875 , 54	825 , 59
	20.5	972 , 42	908 , 47	900 , 45	849 , 59
Iron	14.0	370 , 36	366 , 38	357 , 32	346 , 32
	14.5	420 , 34	414 , 35	407 , 33	390 , 30
	15.0	461 , 34	464 , 34	452 , 31	432 , 29
	15.5	507 , 32	508 , 34	493 , 28	471 , 26
	16.0	545 , 29	542 , 31	533 , 27	509 , 25
	16.5	582 , 25	577 , 27	568 , 27	544 , 26
	17.0	619 , 23	610 , 29	600 , 25	577 , 24
	17.5	652 , 22	641 , 26	631 , 25	609 , 22
	18.0	688 , 21	668 , 24	660 , 25	640 , 24
	18.5	720 , 18	697 , 21	689 , 24	669 , 23
	19.0	754 , 18	725 , 22	717 , 21	701 , 20
	19.5	787 , 17	754 , 21	744 , 20	730 , 21
	20.0	820 , 16	783 , 19	774 , 20	759 , 21
	20.5	853 , 14	809 , 19	802 , 20	791 , 22

References

[1] S. Swordy and D. Kieda, “Elemental Composition of Comic Rays near the Knee by Multiparameter Measurments of Air Showers”, submitted to Astropart. Phys. (1999).

[2] Cortina *et al*, “Cherenkov Light based Measurement of the Chemical Composition and Energy Spectrum of Cosmic Rays with the HEGRA Detector”, *Proc. of the 25rd Int. Cosmic Ray Conf. (Durban),* **4** (1997) 69.

[3] D. J. Bird *et al*, “Evidence for Correlated Changes on the Spectrum and Composition of Cosmic Rays at Extremely High Energies”, PRL **71** (1993) 3401.

[4] T. Abu-Zayyad *et al*, ”The Prototype High Resolution Fly’s Eye Cosmic Ray Detector” submitted to NIMA (1999).

[5] The Auger Collaboration, “The Pierre Auger Project — Design Report”, FNAL, revised March 1997.

[6] D. Knapp *et al*, “CORSIKA: A Monte Carlo Code to Simulate Air Showers”, Forschungszentrum Karlsruhe Report FZKA 6019 (1998).

J. Knapp, D. Heck and G. Schatz, “Comparison of Hadronic Interaction Models Used in Air Shower Simulations and Their Influence on Shower Development and Observables”, Forschungszentrum Karlsruhe Report FZKA 5828 (December 1996).

J. Knapp, D. Heck and G. Schatz, “Inelastic Cross Sections and Their Influence on Air Shower Development”, Forschungszentrum Karlsruhe (June 1997).

J. Knapp and D. Heck, “Extensive Air Shower Simulation with CORSIKA: A User’s Guide”, Forschungszentrum Karlsruhe.

Available at `http://www-ik3.fzk.de/~heck/corsika/`

[7] W.R. Nelson, H. Hirayama, D.W.O. Rogers, “The EGS4 Code System”, Report **SLAC 265** (1985), Stanford Linear Accelerator Center.

[8] H. Fesefeldt, Report **PITHA-85/02** (1985), RWTH Aachen.

[9] D. Heck and J. Knapp, "Upgrade of the Monte Carlo Code CORSIKA to Simulate Extensive Air Showers with Energies $> 10^{20}$ eV", Forschungszentrum Karlsruhe. Report FZK6067B (Draft April 98).

[10] R. Fletcher *et al*, "Sibyll: An Event Generator for Air Shower Simulations", Phys. Rev. D **50** (1994) 5710.

[11] N.N. Kalmykov *et al*, "Quark-Gluon-String Model and EAS Simulation Problems at Ultra-High Energies", Nuc. Phys. B (Proc. Suppl.) **52B** (1997) 17.

[12] A.M. Hillas, *Proc. of the 17th Int. Cosmic Ray Conf. (Paris),* **8** (1981) 193.

A.M. Hillas, "The MOCCA program: MOnte Carlo CAscades", *Proc. of the 24th Int. Cosmic Ray Conf. (Rome),* **1** (1995) 270.

[13] T.K. Gaisser and A.M. Hillas, "Reliability of the Method of Constant Intensity Cuts for Reconstruction of the Average Development of Vertical Showers", *Proc. of the 15th Int. Cosmic Ray Conf. (Plovdiv),* **8** (1977) 353.

[14] M. Goosens *et al*, "HBOOK Refernce Manual", *CERN*, Geneva Switzerland, (1995) page 103.

[15] T. K. Gaisser *et al*, "Cosmic-ray composition around 10^{18} eV", Phys. Rev. D. **47** (1993) 1919.

[16] B. R. Dawson *et al*, "A Comparison of Cosmic Ray Composition Measurements at the Highest Energies", submitted to Astropart. Phys. (1998).

[17] D. J. Bird *et al*, "The Cosmic Ray Composition Above 0.1 EeV", *Proc. of the 23rd Int. Cosmic Ray Conf. (Calgary),* **2** (1993) 38.

[18] "Measurements of Cosmic Ray Air Shower Development at Energies above 10^{17} eV", M. Cassidy *et al*, Ap. J. **356** (1990) 669.

[19] F. Kakimoto *et al*, "A measurement of the air fluorescence yield", NIMA **372** (1996) 527.